Journal of Nuclear Medicine, published on June 6, 2019 as doi:10.2967/jnumed.119.228510

A fully automatic technique for precise localization and quantification of Amyloid-β PET scans

Mouna Tahmi[1*], Wassim Bou-Zeid[1*], Qolamreza R. Razlighi[1, 2]

[1]Department of Neurology, Columbia University Medical Center, New York, NY, United States

[2] Department of Biomedical Engineering, Columbia University, New York, NY, United States

Corresponding author

Mouna Tahmi, MD

Post-doctoral Research Fellow

Email: mt3288@cumc.columbia.edu

Phone 212-342-1330/fax 212-342-1838

↵* Contributed equally to this work.

Financial support: This work has been funded with NIH-NIA R01 AG057962 grant and Taub Institute MRI pilot platform seed award

Running title: Quantification method for Amyloid-β

ABSTRACT

Spatial heterogeneity in the accumulation of Amyloid-β plaques throughout the brain during asymptomatic as well as clinical stages of Alzheimer's disease (AD) calls for precise localization and quantification of this protein using Positron Emission Tomography (PET) imaging. To address this need, we have developed and evaluated a technique that quantifies the extent of Amyloid-β pathology on a millimeter-by-millimeter scale in the brain with unprecedented precision using data from PET scans. **Methods:** An inter-modal, and intra-subject registration with information theoretic cost function was utilized to transform all FreeSurfer neuroanatomical labels into PET image space, which were subsequently used to compute regional standardized uptake value ratio (SUVRs). We have evaluated our technique using post-mortem histopathological staining data from 52 older participants as the standard of truth measurement. **Results:** Our method resulted in consistently and significantly higher SUVRs in comparison to the conventional method in almost all regions of interest. A two-way ANOVA revealed a significant main effect of method as well as a significant interaction effect of method on the relationship between computed SUVR and histopathological staining score. **Conclusion:** These findings suggest that processing the Amyloid-β PET data in subjects' native space can improve the accuracy of the computed SUVRs, as they are more closely associated with the histopathological staining data than the results of the conventional approach.

INTRODUCTION

To quantify the aggregation of brain amyloid-β (Aβ) *in-vivo*, different Aβ tracers have been developed for positron emission tomography (PET) imaging technique, with both clinical and research applications. Aβ PET scans can be evaluated qualitatively through visual reading of the tracer uptake in cortical regions by a trained radiologist (*1*), or quantitatively using automated or semi-automated localization methods to evaluate regional levels of tracer uptake (*2*,*3*). The quantitative methods typically involve localization of tracer uptake in different regions, relative to their uptake in a reference region (ideally a region with little or no specific binding) in the PET scan; this ratio is often refered to as the regional standardized uptake value ratio (SUVR) (*4–6*). Therefore, any inaccuracies in the regional delineation of the PET scan will result in direct quantification error of the computed tracer uptake values. Specifically, such inacuraccies could have detrimental effects on longitudinal Aβ imaging studies, which aim to track small changes in tracer uptake values over time (*7*,*8*). Furthermore, recent studies have demonstrated significant spatial heterogeneity in the regional pattern of Aβ deposition in the brain and its spatial relationship with other brain measures, such as cortical gray-matter thickness and resting-state functional connectivity, in both healthy and clinical populations (*9*,*10*). Taken together, these studies highlight the significant role and clinical importance of varying topographical levels of Aβ deposition, reinforcing the need for precise localization and quantification of this protein in the brain using Aβ PET scans.

The majority of automatic quantifiation methods of Aβ use *spatial normaization* to align/warp all subjects' brain to a standardized template space, presumably making any voxel or region in each subject's brain comparable across all subjects in the study (*11–13*). The limited accuracy of conventional *spatial normalization* methods has been shown in other neuroimaging modalities by

our group (*14*,*15*) and others (*16*,*17*), particularly for older subjects who generally have significant brain atrophy even in the absence of age-related disease (*18*). For example, Video-1 in supplementary materials demonstrates the severity of regional variability in 30 healthy and older brains after being warped to a template space using even the state-of-the-art spatial normalization.

In the present study, our aim is to address the issues associated with inaccurate spatial normalization in automatic quantification of PET scans. By circumventing the *spatial normalization* step and localizing tracer uptake within each subject's brain independently, we propose a *native space* automatic quantification method that reduces the complexity of the between-subject warping problem to a within-subject rigid-body alignment. We used the FreeSurfer parcellation and segmentation (*19*) tool to accurately delineate each region of interest (ROI) in subjects' native space. Then, we transferred the FreeSurfer regional mask to PET space and obtained SUVR data in each FreeSurfer region. We evaluated the accuracy of regional tracer uptake in 52 older participants who had completed both MRI and ^{18}F-Florbetaben PET scans before death, and who also had postmortem assessment of Aβ deposition in their brain using standardized histopathological staining, considered to be standard of the truth (SOT) in this study.

MATERIALS AND METHODS

Participants

The data for the present study were collected during a phase III ^{18}F-Florbetaben PET imaging study conducted from Feb 2010 through July 2013 (*20*), where 52 older subjects (mean ± std age 79.6±9.7, age range: 58-98 years) completed both ^{18}F-Florbetaben PET and MR scans *in-vivo* prior to post-mortem histopathological examination. All subjects (or their legal representatives)

provided written informed consent to undergo a brain MRI and PET with ^{18}F-Florbetaben scans, and also to donate their brains after death to undergo postmortem examination.

^{18}F-Florbetaben Imaging Acquisition

^{18}F-Florbetaben was donated by Piramal (Piramal Pharma Inc.). Detailed information on ^{18}F-Florbetaben PET data acquisition can be found in a previous report describing the phase III ^{18}F-Florbetaben prospective study (*20*). Briefly, PET scans were acquired from participants 90 to 110 minutes after receiving an intravenous injection of 300 MBq ±20% (10 mCi) of ^{18}F-Florbetaben. Reconstruction used an ordered-subset expectation-maximization algorithm, with attenuation correction, scatter, and random correction applied to each of the four 5-minute PET frames acquired.

Structural MRI Acquisition Parameters

Each subject in the study completed a T_1-weighted structural MRI scanning session before death using a 1.5 Tesla magnet and without any exogenous contrast enhancement. An accompanying T_1-weighted magnetization-prepared rapid gradient-echo (MPRAGE) structural whole brain scan (TR/TE = 5~11/2~6 ms; FOV = 25.6 × 16~25.6 cm; matrix size = 256 × 160~256; voxel size = 1.0 × 1.0 × 1.2 mm) was collected for localization and spatial normalization of the PET scans for each participant.

Structural MRI Image Processing

Structural T_1-weighted scans were reconstructed using the FreeSurfer processing pipeline (http://surfer.nmr.mgh.harvard.edu/) to parcellate cortical, and segment subcortical, ROIs. Briefly, structural images were bias field corrected, intensity normalized, and skull stripped using a watershed algorithm, followed by a white matter-based segmentation, defining gray/white matter and pial surfaces, and topology correction (*21*). In total, 95 ROIs masks (35x2 cortical, 23

subcortical, and cerebellar gray and white matter) were extracted from the structural T_1-weighted scan. Based on the availability of the histopathological assessment in specific regions, seven non-overlapping ROIs were selected to compute regional SUVRs: caudal and rostal middle frontal, caudal anterior cingulate, posterior cingulate, precuneus, hippocampus, parahipoccampal gyrus, and lateral occipital cortex. Supplemental Table. 1 lists the regions in which we have the histopathology data available, alongside their corresponding FreeSurfer regions.

Histopathological Staining Procedure

Brain samples from participants who passed away during the study (52 participants) were used to obtain histopathological confirmation of Aβ presence and density in the brain, as previously described in (*20*). Briefly, postmortem histopathologic examination was assessed according to the 4 histologically-defined Consortium for Establishing a Registry for Alzheimer Disease (CERAD) scores (*22*). The onsite pathologist conducted the autopsy within 36 hours of death, and performed the scoring. Tissue was classified as 1 for "absent", 2 for "sparse", 3 for "moderate" or 4 for "frequent" depending on the neuritic plaque densities, as detected by Bielschowsky silver staining. Eight brain regions were dissected, including the middle frontal gyrus, anterior cingulate cortex, posterior cingulate cortex, precuneus, hippocampus, parahippocampal gyrus, occipital cortex and whole cerebellum.

Native Space Method of Quantification

A flowchart of the steps in the proposed native space method has been illustrated in (Fig. 1) The first step in the "native space" method is to create a static PET image by aligning the four dynamic PET frames to the first frame using rigid-body registration to correct for potential head motion during the imaging session (6 degrees-of-freedom, correlation) as seen in Fig. 1A. Subsequently, these four registered frames are averaged together (voxel-wise operation) to create

one static PET image (Fig. 1B). In addition, our proposed method takes advantage of the existing CT scan (often required for attenuation correction in PET) to further improve the accuracy of inter-modal registration, since the information of the subject's skull is completely lost in PET scans, but is visible in CT scans. The static PET and CT scans are co-registered using a rigid body inter-modal registration (6 degrees-of-freedom, normalized mutual information) and merged to generate a composite image in PET static space (Fig. 1C).

Each participant's structural T_1-weighted scan in FreeSurfer space is also registered to the participant's merged image using rigid body registration (6 degrees-of-freedom, normalized mutual information) to obtain the second transformation matrix. A combination of the two transformation matrices is used to transfer the regional masks (ROIs) (including the cerebellum) from FreeSurfer space to static PET image space. The SUVR map was generated by normalizing each voxel's uptake to the averaged uptake in a reference region, which in our study was the whole cerebellum. For the purposes of the present study, SUVRs were calculated within the seven aformentioned cortical ROIs in which the histopathological examination was also performed.

Standard Space Quantification

To compare our proposed native space quantification method to the commonly used conventional method in the field, we also computed the SUVR measurments in the seven selected ROIs using a standard space method that uses the Montreal neurological institute (MNI) template and the automated anatomical labeling (AAL) atlas (*23*). In the standard space method, we first generated static PET image from four dynamic scans as described in the *native space* method. We then registered each participant's static PET scan to their T_1-weighted MRI scan using rigid body transformation (6 degrees-of-freedom, correlation) (Fig. 2B). Tissue segmentation was also performed on each subject's MRI scan to obtain the whole-brain gray-matter tissue mask (Fig.

2C). Next, the T_1-weighted structural MRI scan was registered to the MNI template using a state-of-the-art non-linear registration technique called advanced normalization tools ANTs (*24*,*25*) (Fig. 2B). The combination of the transformations and warping field was then applied to the PET image, generating a spatially normalized PET image in MNI template space, as well as a spatially normalized whole-brain gray matter mask. The intersection of the ROI masks in the AAL atlas with the whole-brain gray matter mask generated the regional mask which was then used to compute regional SUVRs by dividing the average regional uptake within each ROI by that of the whole cerebellum, as obtained directly from the AAL atlas. In addition, to evaluate our method using matching ROIs, we have also repeated the standard space technique using the FreeSurfer generated ROIs in the MNI template space.

Overall Quality Assessment of Registration

Both registration and segmentation algorithms are susceptible to large misalignments. In some cases, even the orientation of the images can be mis-matched. To make sure our results were not driven by these bulk misalignments, we visually inspected the quality of the registration and segmentation in both native space and standard space. We found no major misalignment in native or standard space methods.

Statistical Analysis

All statistical analysis in this work was performed using Microsoft Excel and the JMP 14.0 statistical software package for Microsoft Office. A two-way analysis of variance (ANOVA) including all subjects was conducted to test the effect of the two independent variables (method: *native space* versus *standard space*; and histopathological staining scores: 1 for "absent", 2 for "sparse", 3 for "moderate" or 4 for "frequent") and their interaction on the SUVR measurements. This analysis was performed for both aggregated data by combining data from all seven available

regions, as well as for each region separately. Post-hoc Student's t-tests were performed to further prove the effect of normalization method at each level of the histopathological staining. Difference in slope tests were used as secondary post-hoc tests to examine the interaction effects on every region, as well as on the aggregated data. Higher slopes should indicate a stronger correlation, or predictive power, between the measured SUVRs and histopathological staining scores. Finally, standard F-tests were used to assess any difference in SUVR variance obtained from the two methods.

RESULTS

Table 1 summarizes the demographics of the 52 participants who were scanned with ^{18}F-Florbetaben and underwent post-mortem histopathological evaluation for Aβ burden. Of the 52 participants, 33 (63.5%) were classified as probable AD, 12 (23%) as other dementia patients, 7 (13.5%) classified as non-demented volunteers. There were no significant differences between the three groups in age or sex ($t_{age}< 1.7$, $p_{age}>0.07$; $t_{sex}< 1.34$, $p_{sex}>0.2$)

A two-way ANOVA (factors: method and histopatholoical score) test performed on the aggregated data showed a main effect of method (F=198.80, P=<0.0001), a main effect of histopathological staining score (F=87.73, P=<0.0001), and a significant method × histopathology interaction (F=6.43, P=0.0114). We then explored these significant findings further: first, by investigating the main effect of method. Table 2 lists the results of Student's t-tests for two independent SUVR measurements, indicating whether the two methods generated significantly different SUVRs for each histopathological staining score within each region. As evident from these results, the mean SUVR values were significantly higher for the *native space* method compared to the standard method (Avg. $SUVR_{Diff}$=0.29, t_{paired}=12.64, P<0.0001). The difference in the mean SUVRs were also signifcant for all seven selected brain regions, and every

corresponding histopathological level ($t>2.5$, $P<0.05$), except middle frontal level 3 ($t=1.93$ $P=0.06$) and occipital level 2 ($t=1.99$ $P=0.056$), which were only marginally significant. Fig. 4 also illustrates these differences in mean SUVR using boxplots. Overall, the precuneus, posterior cingulate and anterior cingulate showed higher SUVR values compared to the rest of the regions.

Next, to investigate the interaction between method and histopathological score, we conducted a difference in slope test between the two methods in the aggregated dataset, as well as in the seven preselected ROIs. As seen in Fig. 3, the *native space* method improved the slope of the relationship between histopathological score and SUVR measurement significantly compared to the *standard space* method ($\beta_{diff}=0.05$, $P< 0.01$) in the aggregated data. We then looked at this effect in the different regions separately. As seen in Fig. 4, overall, slopes were higher in the *native space* compared to the standard method in all seven ROIs. Native space results showed a significant positive slope in six of the seven selected ROIs ($\beta>0.049$, $P<0.009$) with one non-significant slope in the hippocampus ($\beta=0.02$, $P=0.25$). On the other hand, using the standard space method, only four out of seven ROIs showed a significant positive slope ($\beta>0.039$, $P< 0.012$). Furthermore, the regional slope difference tests between the two methods were significant in the precuneus ($\beta_{diff}=0.1$, $p=0.028$) and posterior cingulate gyrus ($\beta_{diff}=0.121$, $p=0.017$), while the slope difference tests for the rest of the regions did not reach significance (Fig. 4).

We also performed F-tests to assess any significant differences in variance associated with each histopathological stage in each region for both methods (Supplemental Table. 2). The results of the F-tests revealed no significant differences in all regions and their corresponding histopathological levels, except for four cases in which the native space method resulted in either lower variance (hippocampus stage 4; $f=0.23$, $p=0.02$) or higher variance (posterior cingulate stage 2, occipital stage 1 and 3; $f>3.13$, $p<0.03$). In addition, repeating the standard space method using

the FreeSurfer regions in MNI space instead of the AAL atlas did not improve its results. Supplemental Fig. 1 illustrates the results of this analysis, where the native space method outperformed the standard space method in four out of seven ROIs (precuneus, posterior cingulate, anterior cingulate, middle frontal). Since the results of native space have not been altered, this must mean that the standard space results with FreeSurfer regions have substantially lower correlation with histopathological score in comparison to standard space results with AAL atlas ROIs.

DISCUSSION

The goal of this study was to introduce and evaluate our *native space* technique in quantifying Aβ accumulation as imaged by ^{18}F-Florbetaben PET scans in comparison to the *standard space* approach commonly used to analyze Aβ PET data (*20*,*26*). Our findings suggest that the *native space* method using FreeSurfer's parcellation and segmentation outperformes the *standard space* approach based on the MNI template and AAL atlas. Considering the histopathological assessment as the SOT for Aβ quantification, we show that the SUVR measurments obtained through the *native space* method are not only significantly higher than the ones obtained through the *standard space* method in almost all available brain regions and every histopathological staining level, but they are also significantly more predictive of the histopathological staining scores, suggesting higher precision of Aβ quantification.

Recently, and in line with our work, Schwarz et al. (*27*), investigated the effects of imprecise rigid-body registration between Aβ PET and MRI on SUVR measurement. The authors reported that imprecision in PET-MRI rigid-body registration contributes to imprecise change over time measurements by approximately 7% of the expected reference values for annual change in subjects

with AD pathology. According to the authors, this imprecision increases with Aβ load. Brain Aβ aggregation on the other hand, reflects significant spatial heterogeneity. Frontal, posterior cingulate, and precuneus regions have been widely reported as regions with the highest levels of Aβ deposition in AD brains (*6*,*20*,*28*). More importantly, studies looking at Aβ deposition in early AD as well as in mild cognitive impairment have shown that these regions are areas of initial Aβ deposition, suggesting that deposition starts in these regions, and continues to accrue as the disease progresses (*29*,*30*). Interestingly, and in light of the results of the current study, the posterior cingulate and precuneus were regions in which the native space method demonstrated higher and significant correlations with histopathology, as well as the most significant improvement in the precision of Aβ quantification when compared to the standard space method. Thus, the native space method could potentially enhance the ability to detect Aβ in the preclinical phases of AD, which is of importance as there is growing interest in detecting Aβ earlier in life, as well as undersatnding the progression of its deposition *in vivo* (i.e., Grothe's Aβ imaging staging (*31*)).

The native space SUVR from the hippocampus did not show any relationship with histopathological staging scores. This may raise the concern that for quantifying SUVRs within smaller regions, the native space method might not be as effective as it is for larger regions. However, we argue that this is, in fact, not the case. First, unlike results using the conventional method, the native space SUVR for the parahippocampal region (a brain region with similar size in the medial temporal lobe) shows a significant relationship with histopathological staging scores. Second, the hippocampal regions in the brain are shown to lack sensitivity for Aβ compared to the other regions included in the present study (*20*). Third, the conventionally-computed SUVRs from the hippocampus, as well as from the parahipocampus regions, are quite low (SUVR $<<$ 1 for all four staining scores), which indicates that Aβ deposition in these regions is much lower than that

in the reference region (presumably with no Aβ deposition), suggesting that the SUVRs computed using the standard space method are biased toward lower SUVRs. Finally, one can expect that the level of imprecision in ROI delineation (particularly in small regions) using the standard space method could have a large effect on corresponding SUVR values. Due to these reasons, we think that the effectiveness of the native space method is likely not altered in smaller regions, and that the reason for this lack of relationship between native space computed SUVRs and histopathological staining scores in the hippocampus is, in fact, due to the lack of significant Aβ deposition.

We have used the proposed method in previously published studies in our division (*32–34*), however the actual evaluation of our method using standard of truth has not been performed previously. In our previous studies, our analysis pipeline took advantage of the existing CT scan, which has the registration advantage of showing skull bone structure. In the current study, CT data were unfortunately missing from the imaging dataset that was used, however we still had significant improvement of SUVR measurement compared to the standard method. Hence, we are confident that if CT data were available, our results would be only more robustly in favor of the native space method.

It is noteworthy that other MRI template spaces (e.g. Talairach space) and/or atlases can be used in the standard space method, as shown in previous research including ^{18}F-Florbetaben PET (*4*,*6*). However, all standard space methods are based on spatial normalization, which requires non-linear registration of data to a standard template. Therefore, we expect that SUVR values produced using these other template methods to have a similar degree of imprecision compared to the native space method in which there is no need for spatial normalization. Repeating our analysis for the standard method using the FreeSurfer regions in MNI space to ensure the comparability of ROIs

between native space and the standard method did not improve the results of the standard space method, and native space still outperformed the standard space with the FreeSurfer labels in four out of seven ROIs (Supplemental Fig.1). We think that the reason the standard space method with FreeSurfer labels did not improve the results is because: 1) The cortical regions in the FreeSurfer atlas from MNI space are relatively thin, therefore even a small mis-alignment or inaccuracy in spatial normalization would completely shift the ROI to white-matter or CSF, whereas the AAL atlas, which not only covers gray matter but also a large portion of the white matter and CSF, could be less sensitive to such a small mis-alignment; and 2) In our native space method, we use a grey matter mask obtained by a whole-brain tissue segmentation tool, as done in previous studies (*26*,*35*), to exclude binding in white matter and CSF. We did not compare our method to other MR-free quantification methods which are based on PET-to-PET registration to a common template (*2*,*36*) due to the fact that MRI is largely acquired in PET quantification studies, as well as in clinical trials of AD. Only large-scale studies evaluating all other template approaches (MR-based or MR-free), using *in vivo* Aβ PET alongside post-mortem histopathological assessment will be able to assess the complete effect of all methods of spatial normalization on Aβ PET data validity.

It should be noted that our method was only applied to Aβ PET data obtained using the ^{18}F-Florbetaben tracer. We did not test this method using other Aβ PET tracers such as the Pittsburgh Compound B (^{11}C-PIB), and other ^{18}F-labeled tracers (^{18}F-Florbetapir and ^{18}F-Flutemetamol). These tracers also use SUVR quantification, typically computed through a process that involves registration of the PET scan to a standard space using spatial normalization. Thus, while the present study only includes PET data obtained using the ^{18}F-Florbetaben tracer, it is expected that spatial normalization would significantly affect the accuracy of PET data obtained using any of the

available Aβ PET tracers. However, future studies should formally assess whether the standard space method has similar effects on data from all amyloid PET tracers.

Nowadays it is a common practice to collect neuroimaging data from multiple centers for large clinical studies/trials. Reducing between-center variability continues to be an issue for multi-center studies/trials, so it would be beneficial to assess whether utilization of the native space method would mitigate or exacerbate multi-center variability/noise. Using the center information in the Piramal Phase III dataset to conduct a one-way ANOVA of the effect of center on SUVRs, we have detected significant center-related variability in the standard space SUVRs acquired from different sites ($f=2.12$, $p<0.01$), which was significantly attenuated by using the native space method ($f=1.18$, $p=0.33$). Together these findings suggest that using the native space method could potentially reduce the variability due to acquiring data from different sites in the computed SUVRs, which could also be beneficial in processing multi-center PET data. However, further investigation using a much larger sample is required to properly investigate this effect in the future. Furthermore, future research must assess the impact of the native space method on SUVR measurement precision in other datasets such as the ^{18}F-Florbetaben test-retest scans (*37*), which would be critical for use of amyloid PET as a treatment endpoint in anti-amyloid clinical trials. Additionally, in order to directly compare results across studies, another future study should test the effect/benefit of native space method, in comparison to a spatially-normalized method, in the ^{18}F-Florbetaben centiloid datasets (*38*).

Finally, we are aware of the fact that the degree of precision of SUVR measurement in Aβ PET imaging can also be affected by other factors such as the choice of the reference region, the type of Aβ tracer, scan duration relative to injection timing, size of ROIs, and use of partial volume correction, all of which have been widely addressed in previous studies (*8*,*39*,*40*). In this work,

our automatic quantification method specifically focuses on the effect of an under-studied SUVR measurement factor, spatial normalization, which subsequently affects the precision of ROI localization. Luckily, spatial normalization is a post-processing step that can be easily eliminated, as is the case using our native space approach, and can even be applied to existing Aβ PET data, which therefore could improve the precision of SUVR measurement in past studies retrospectively.

CONCLUSION

We have highlighted the inaccuracy of the regional SUVR measurments obtained from the quantification of Aβ PET scans with ^{18}F-Florbetaben tracer using the conventional standard space technique. We proposed a more accurate quantification method by circumventing the problematic non-linear registration step and processing the PET scans in subjects' native space. We evaluated our proposed method by showing that native space regional SUVRs are more closely related to standardized histopathological staging scores than the regional SUVRs computed using the conventional standard space technique. This analysis approach could especially benefit studies targetting early detection and regional differenciation of brain amyloid burden, which is important especially in view of the regional heterogeneity in brain Aβ deposition.

DISCLOSURE

This work has been funded with NIH-NIA R01 AG057962 grant and Taub Institute MRI pilot platform seed award. No potential conflicts of interest relevant to this article exist.

ACKNOWLDGMENTS

Special thanks to Andrew Stephens, Susan De Santi, Santi Bullich, and Osama Sabri in Life Molecular Imaging (formerly known as Piramal) for providing MRI, PET, and histopathological

scoring data, Hengda He for preparing boxplot figures, and Eleanna Varangis for her proof reading of the manuscript.

KEY POINTS

Question: Does analyzing brain Amyloid-β PET imaging in subjects' native space (without spatial normalization) improve the accuracy of the resulting SUVRs compared to the same analysis in standard space (with spatial normalization)?

Pertinent finding: Using our native space method resulted in significantly higher measurement precision of Amyloid-β compared to a commonly used standard method that relies on spatial normalization.

Implications for patient care: Our method can be applied to existing or future Amyloid-β PET data to improve the accuracy of SUVRs, especially when tracking small changes in deposition over the course of Alzheimer's pathology.

REFERENCES

1. Seibyl J, Catafau AM, Barthel H, et al. Impact of Training Method on the Robustness of the Visual Assessment of 18F-Florbetaben PET Scans: Results from a Phase-3 Study. *J Nucl Med*. 2016;57:900-906.
2. Joshi AD, Pontecorvo MJ, Lu M, Skovronsky DM, Mintun MA, Devous MDS. A Semiautomated Method for Quantification of F 18 Florbetapir PET Images. *J Nucl Med*. 2015;56:1736-1741.
3. Zubal G, Wisniewski G, Seibyl J. Automated software package for analyzing new beta-amyloid radioligands in Alzheimer's patients. *J Nucl Med*. 2008;49:378P-378P.
4. Fleisher AS. Using Positron Emission Tomography and Florbetapir F 18 to Image Cortical Amyloid in Patients With Mild Cognitive Impairment or Dementia Due to Alzheimer Disease. *Arch Neurol*. 2011;68:1404-1411.
5. Jack CR, Lowe VJ, Senjem ML, et al. 11C PiB and structural MRI provide complementary information in imaging of Alzheimer's disease and amnestic mild cognitive impairment. *Brain*. 2008;131:665-680.
6. Villemagne VL, Ong K, Mulligan RS, et al. Amyloid Imaging with 18F-Florbetaben in Alzheimer Disease and Other Dementias. *J Nucl Med*. 2011;52:1210-1217.
7. Landau SM, Breault C, Joshi AD, et al. Amyloid- Imaging with Pittsburgh Compound B and Florbetapir: Comparing Radiotracers and Quantification Methods. *J Nucl Med*. 2013;54:70-77.
8. Schmidt ME, Chiao P, Klein G, et al. The influence of biological and technical factors on quantitative analysis of amyloid PET: Points to consider and recommendations for

controlling variability in longitudinal data. *Alzheimers Dement*. 2015;11:1050-1068.

9. Mormino EC, Smiljic A, Hayenga AO, et al. Relationships between beta-amyloid and functional connectivity in different components of the default mode network in aging. *Cereb Cortex*. 2011;21:2399-2407.
10. Doherty BM, Schultz SA, Oh JM, et al. Amyloid burden, cortical thickness, and cognitive function in the Wisconsin Registry for Alzheimer's Prevention. *Alzheimer's Dement (Amsterdam, Netherlands)*. 2015;1:160-169.
11. Talairach, J. and Tournoux P. Co-planar stereotaxic atlas of the human brain: 3-dimensional proportional system: an approach to cerebral imaging. New York, NY: Thieme Medical Pub- lishers; 1988.
12. Mazziotta J, Toga A, Evans A, et al. A probabilistic atlas and reference system for the human brain: International Consortium for Brain Mapping (ICBM). *Philos Trans R Soc B Biol Sci*. 2001;356:1293-1322.
13. Camus V, Payoux P, Barré L, et al. Using PET with 18F-AV-45 (florbetapir) to quantify brain amyloid load in a clinical environment. *Eur J Nucl Med Mol Imaging*. 2012;39:621-631.
14. Razlighi QR, Habeck C, Steffener J, et al. Unilateral disruptions in the default network with aging in native space. *Brain Behav*. 2014;4:143-157.
15. Liu X, Gerraty RT, Grinband J, Parker D, Razlighi QR. Brain atrophy can introduce age-related differences in BOLD response. *Hum Brain Mapp*. 2017;38:3402-3414.
16. Seibert TM, Brewer JB. Default network correlations analyzed on native surfaces. *J Neurosci Methods*. 2011;198:301-311.
17. Senjem ML, Gunter JL, Shiung MM, Petersen RC, Jack CRJ. Comparison of different

methodological implementations of voxel-based morphometry in neurodegenerative disease. *Neuroimage*. 2005;26:600-608.

18. Fjell AM, Walhovd KB, Fennema-Notestine C, et al. One-year brain atrophy evident in healthy aging. *J Neurosci*. 2009;29:15223-15231.

19. Fischl B, van der Kouwe A, Destrieux C, et al. Automatically parcellating the human cerebral cortex. *Cereb Cortex*. 2004;14:11-22.

20. Sabri O, Sabbagh MN, Seibyl J, et al. Florbetaben PET imaging to detect amyloid beta plaques in Alzheimer's disease: Phase 3 study. *Alzheimer's Dement*. 2015;11:964-974.

21. Dale AM, Fischl B, Sereno MI. Cortical Surface-Based Analysis. *Neuroimage*. 1999;9:179-194.

22. Mirra SS, Heyman A, McKeel D, et al. The Consortium to Establish a Registry for Alzheimer's Disease (CERAD). Part II. Standardization of the neuropathologic assessment of Alzheimer's disease. *Neurology*. 1991;41:479-86.

23. Tzourio-Mazoyer N, Landeau B, Papathanassiou D, et al. Automated Anatomical Labeling of Activations in SPM Using a Macroscopic Anatomical Parcellation of the MNI MRI Single-Subject Brain. *Neuroimage*. 2002;15:273-289.

24. Klein A, Ghosh SS, Avants B, et al. Evaluation of volume-based and surface-based brain image registration methods. *Neuroimage*. 2010;51:214-220.

25. Avants BB, Epstein CL, Grossman M, Gee JC. Symmetric diffeomorphic image registration with cross-correlation: evaluating automated labeling of elderly and neurodegenerative brain. *Med Image Anal*. 2008;12:26-41.

26. Barthel H, Gertz H-J, Dresel S, et al. Cerebral amyloid-β PET with florbetaben (18F) in patients with Alzheimer's disease and healthy controls: a multicentre phase 2 diagnostic

study. *Lancet Neurol*. 2011;10:424-435.

27. Schwarz CG, Jones DT, Gunter JL, et al. Contributions of imprecision in PET-MRI rigid registration to imprecision in amyloid PET SUVR measurements. *Human Brain Mapping*. 2017;38:3323-3336.

28. Hsiao IT, Huang CC, Hsieh CJ, et al. Perfusion-like template and standardized normalization-based brain image analysis using18F-florbetapir (AV-45/Amyvid) PET. *Eur J Nucl Med Mol Imaging*. 2013;40:908-920.

29. Braak H, Braak E. Neuropathological stageing of Alzheimer-related changes. *Acta Neuropathol*. 1991;82:239-259.

30. Fodero-Tavoletti MT, Rowe CC, McLean CA, et al. Characterization of PiB binding to white matter in Alzheimer disease and other dementias. *J Nucl Med*. 2009;50:198-204.

31. Grothe MJ, Barthel H, Sepulcre J, Dyrba M, Sabri O, Teipel SJ. In vivo staging of regional amyloid deposition. *Neurology*. 2017;89:2031-2038.

32. Oh H, Steffener J, Razlighi QR, et al. Aβ-related hyperactivation in frontoparietal control regions in cognitively normal elderly. *Neurobiol Aging*. 2015;36:3247-3254.

33. Oh H, Steffener J, Razlighi QR, Habeck C, Stern Y. beta-Amyloid Deposition Is Associated with Decreased Right Prefrontal Activation during Task Switching among Cognitively Normal Elderly. *J Neurosci*. 2016;36:1962-1970.

34. Gu Y, Razlighi QR, Zahodne LB, et al. Brain Amyloid Deposition and Longitudinal Cognitive Decline in Nondemented Older Subjects: Results from a Multi-Ethnic Population. *PLoS One*. 2015;10:e0123743.

35. Lilja J, Leuzy A, Chiotis K, Savitcheva I, Sörensen J, Nordberg A. Spatial Normalization of 18 F-Flutemetamol PET Images Using an Adaptive Principal-Component Template . *J*

Nucl Med. 2018;60:285-291.

36. Raniga P, Bourgeat P, Ourselin S, Villemagne V, O'Keefe G, Rowe C. PIB-PET segmentation for automatic SUVR normalisation without MR information. *2007 4th IEEE Int Symp Biomed Imaging From Nano to Macro - Proc*. 2007:348-351.
37. Sabri O, Seibyl J, Rowe C, Barthel H. Beta-amyloid imaging with florbetaben. *Clin Transl Imaging*. 2015;3:13-26.
38. Rowe CC, Doré V, Jones G, et al. 18F-Florbetaben PET beta-amyloid binding expressed in Centiloids. *Eur J Nucl Med Mol Imaging*. 2017;44:2053-2059.
39. Carbonell F, Zijdenbos AP, Charil A, Grand'Maison M, Bedell BJ. Optimal Target Region for Subject Classification on the Basis of Amyloid PET Images. *J Nucl Med*. 2015;56:1351-1358.
40. Landau SM, Fero A, Baker SL, et al. Measurement of longitudinal beta-amyloid change with 18F-florbetapir PET and standardized uptake value ratios. *J Nucl Med*. 2015;56:567-574.

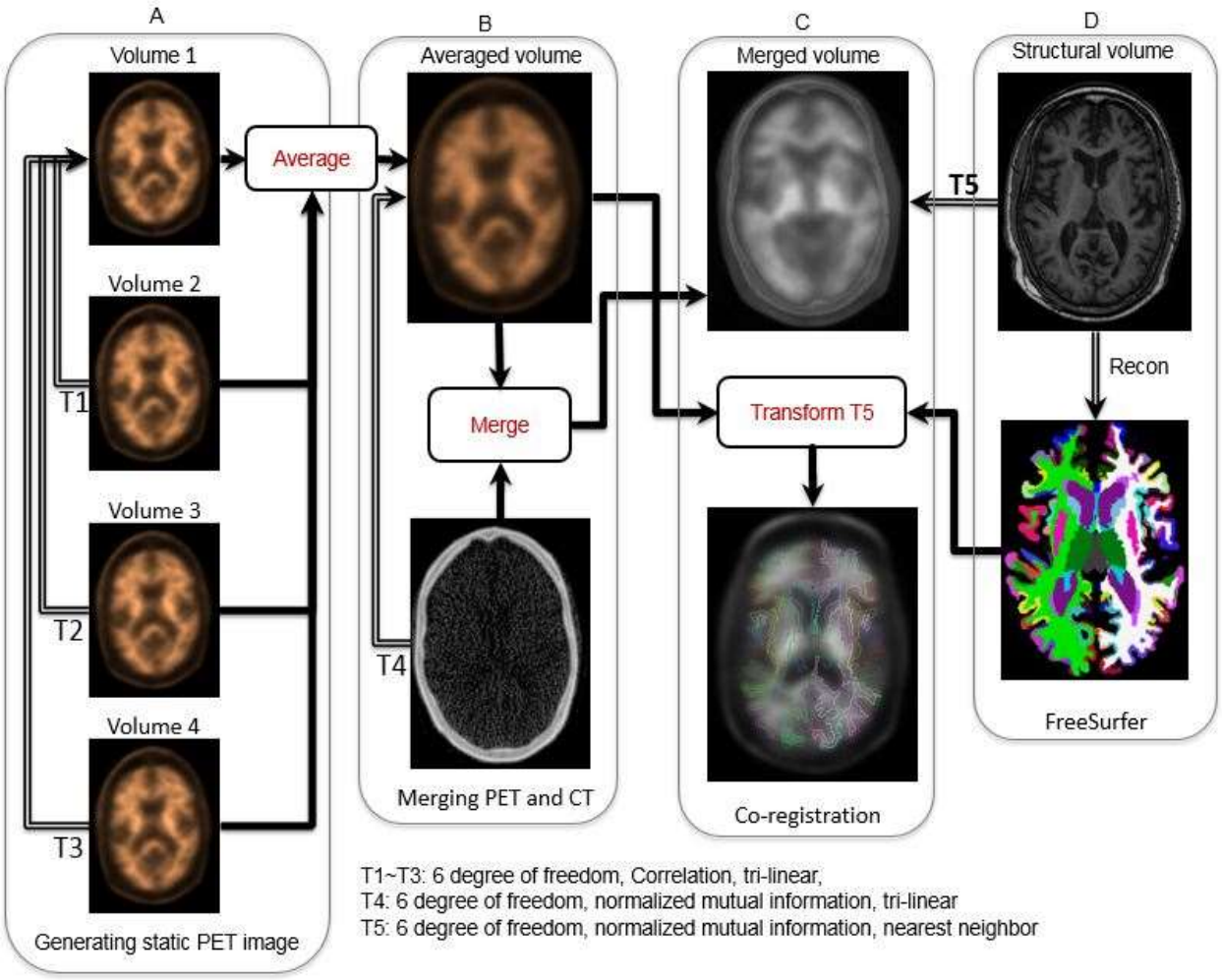

Figure 1. Flowchart of our developed PET image reconstruction technique (native space). (A) Generating static PET image (B) Merged PET and CT (C) Co-registration (D) FreeSurfer segmentation.

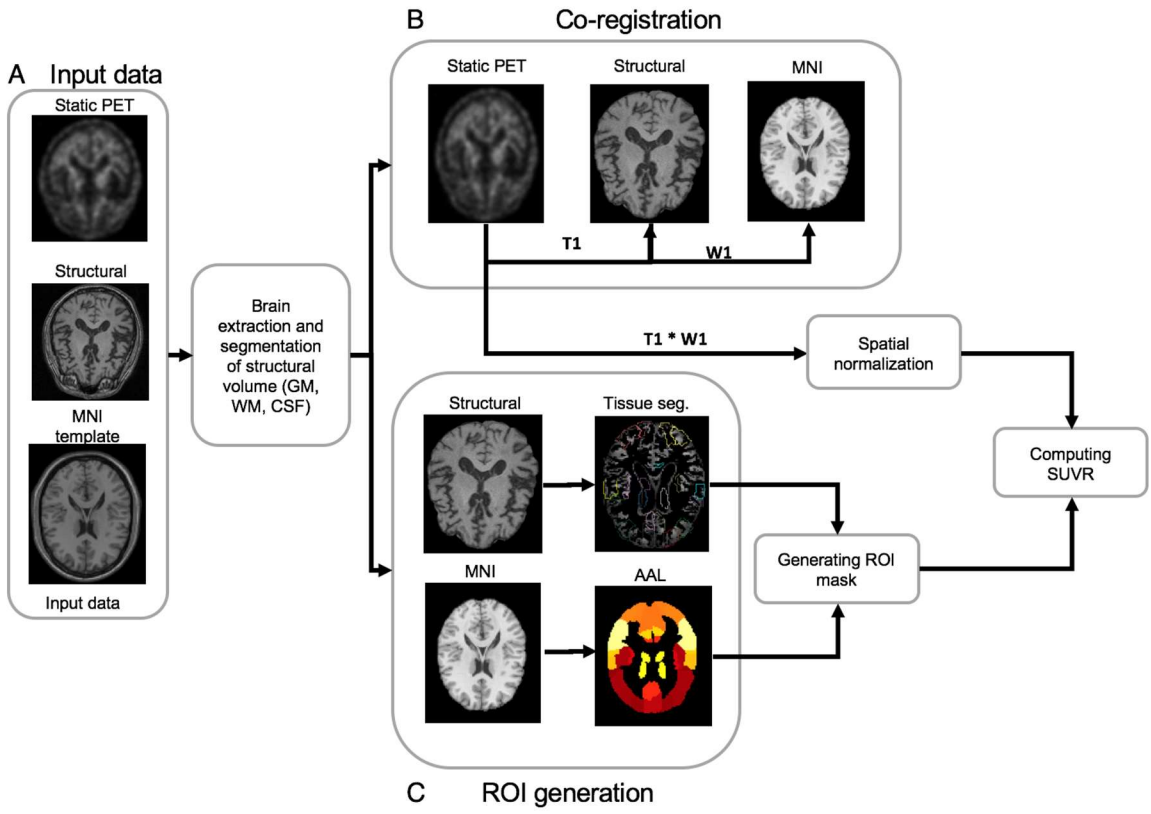

Figure 2. Flowchart of the standard PET image reconstruction technique (standard space method). (A) Input data (B) Co-registration (C) ROI generation

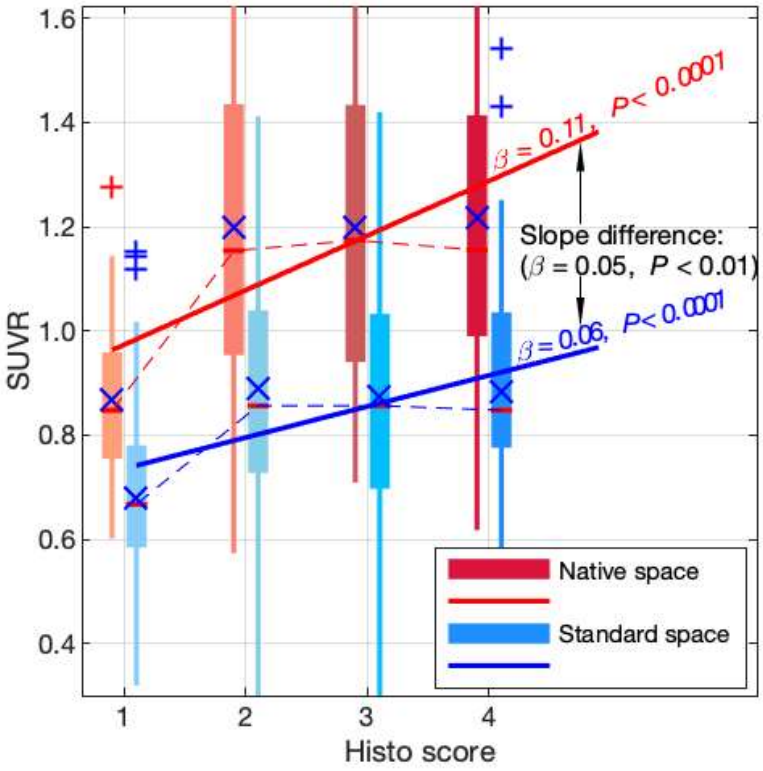

Figure 3. Regression Plot for 2-way ANOVA (Histopathology X Method) on SUVRs. Depicts the significant slope difference between our technique (native) as well as the conventional method (standard) for all regions.

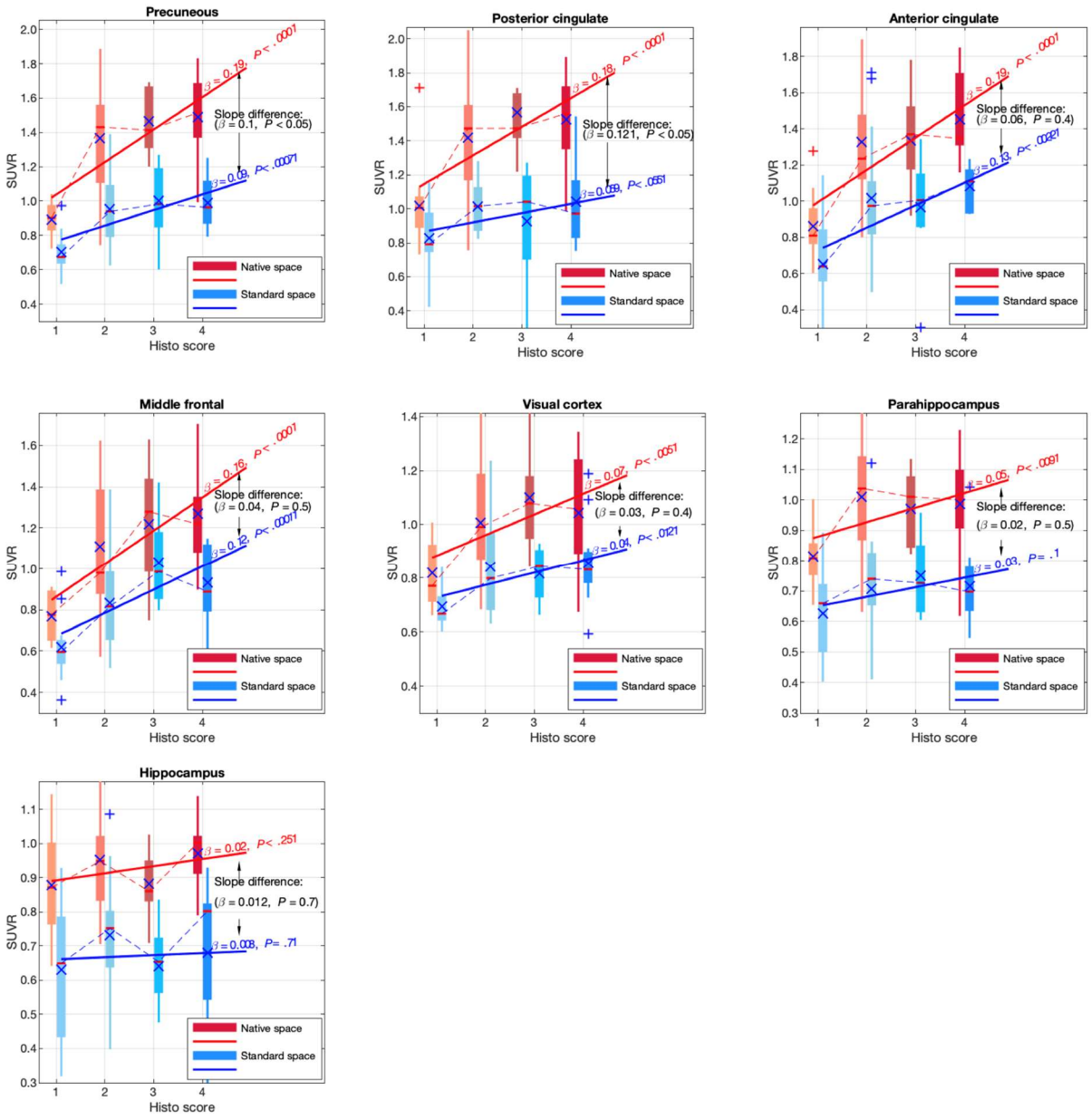

Figure 4. Box and whisker plots with correlation and slope test parameters showing SUVR distribution obtained using native and standard methods based on postmortem histopathological staging**.** Depicts the distribution of regional uptakes obtained from our technique (native) as well as the conventional method (standard) for every level of histopathological staging for each of the seven selected ROIs in separate plots.

Table 1. Demographics of scanned and autopsied research subjects

Parameter	AD (n=33)	Other dementias (n=12)	Non-demented volunteers (n=7)
Age (y)	78.76 ± 10.09	79.67 ± 8.28	87.14 ± 9.84
Sex			
M	20	3	9
F	13	4	3

Table 2. Regional mean and SD of SUVRs for native and standard methods based on pathology levels and t-test results comparing the 2 methods.

ROI	Histo Score	Native SUVR	Standard SUVR	P
Middle frontal	1 (n= 12)	0.77±0.12	0.62±0.17	<0.05*
	2 (n=17)	1.11±0.32	0.83±0.24	<0.01*
	3 (n=13)	1.22±0.29	1.03±0.20	0.06
	4 (n=10)	1.27±0.26	0.93±0.19	<0.01*
Ant Cingulate	1 (n=14)	0.86±0.18	0.65±0.23	0.01*
	2 (n=21)	1.33±0.33	1.01±0.30	<0.01*
	3 (n=10)	1.34±0.26	0.97±0.28	<0.01*
	4 (n=6)	1.45±0.27	1.08±0.13	0.01*
Post Cingulate	1 (n=16)	1.02±0.22	0.83±0.19	0.01*
	2 (n=18)	1.42±0.34	1.01±0.14	<0.001*
	3 (n=8)	1.56±0.29	0.93±0.35	0.001*
	4 (n=9)	1.53±0.29	1.04±0.28	<0.01*
precuneus	1 (n=14)	0.89± 0.1	0.7±0.11	<0.001*
	2 (n=21)	1.37±0.30	0.95±0.2	<0.001*
	3 (n=7)	1.46±0.2	1.00±0.24	<0.01*
	4 (n=9)	1.49±0.27	0.99±0.16	<0.001*
Hippocampus	1 (n=17)	0.88±0.15	0.63±0.19	<0.001*
	2 (n=14)	0.95±0.15	0.73±0.19	<0.01*
	3 (n=12)	0.88±0.09	0.64±0.11	<0.001*
	4 (n=9)	0.97±0.11	0.68±0.22	<0.01*
Parahippocampus	1 (n=17)	0.81±0.1	0.63±0.14	<0.001*
	2 (n=14)	1.01±0.18	0.71±0.21	<0.001*
	3 (n=7)	0.97±0.13	0.75±0.13	<0.01*
	4 (n=11)	0.99±0.17	0.72±0.13	<0.001*
Occipital	1 (n=13)	0.82±0.12	0.69±0.07	<0.01*
	2 (n=14)	1.01±0.23	0.84±0.19	0.056
	3 (n=10)	1.1±0.21	0.82±0.1	0.001*
	4(n=14)	1.04±0.22	0.86±0.15	0.01*

*Significantly higher SUVR mean for the native method compared to the standard method.

Supplemental Table 1. Brain regions derived from the histopathology and their Free Surfer corresponding regions that were employed in our analysis.

Histopathology regions	FreeSurfer regions
Middle frontal	Caudal middle frontal Rostral middle frontal
Anterior Cingulate	Caudal Anterior Cingulate
Posterior Cingulate	Posterior Cingulate
Precuneus	Precunous
Hippocampus	Hippocampus
Parahippocampus	Parahipoccampus
Occipital	Lateral occipital

Supplemental Table 2. F-test results comparing the variance of SUVRs for native and standard method for each pathology level.

ROI	Histo Score	Native SUVR variance	Standard SUVR variance	F test	P
Middle frontal	1 (n= 12)	0.01	0.03	0.53	0.15
	2 (n=17)	0.10	0.06	1.87	0.11
	3 (n=13)	0.08	0.04	2.15	0.10
	4 (n=10)	0.07	0.04	1.90	0.18
Ant Cingulate	1 (n=14)	0.03	0.05	0.63	0.21
	2 (n=21)	0.11	0.09	1.19	0.35
	3 (n=10)	0.07	0.08	0.86	0.41
	4 (n=6)	0.07	0.02	4.24	0.07
Post Cingulate	1 (n=16)	0.05	0.04	1.26	0.33
	2 (n=18)	0.11	0.02	6.13	0.00*
	3 (n=8)	0.08	0.12	0.65	0.29
	4 (n=9)	0.08	0.08	1.06	0.47
precuneus	1 (n=14)	0.01	0.01	0.91	0.43
	2 (n=21)	0.09	0.04	2.17	0.05
	3 (n=7)	0.04	0.06	0.71	0.35
	4 (n=9)	0.07	0.02	2.95	0.07
Hippocampus	1 (n=17)	0.02	0.04	0.63	0.18
	2 (n=14)	0.02	0.04	0.62	0.20
	3 (n=12)	0.01	0.01	0.67	0.26
	4 (n=9)	0.01	0.05	0.23	0.03*
Parahippocampus	1 (n=17)	0.01	0.02	0.54	0.11
	2 (n=14)	0.03	0.04	0.75	0.31
	3 (n=7)	0.02	0.02	0.93	0.46
	4 (n=11)	0.03	0.02	1.58	0.24
Occipital	1 (n=13)	0.01	0.00	3.13	0.03*
	2 (n=14)	0.06	0.04	1.45	0.25
	3 (n=10)	0.04	0.01	4.46	0.02*
	4(n=14)	0.05	0.02	2.19	0.08

*Significantly different variance

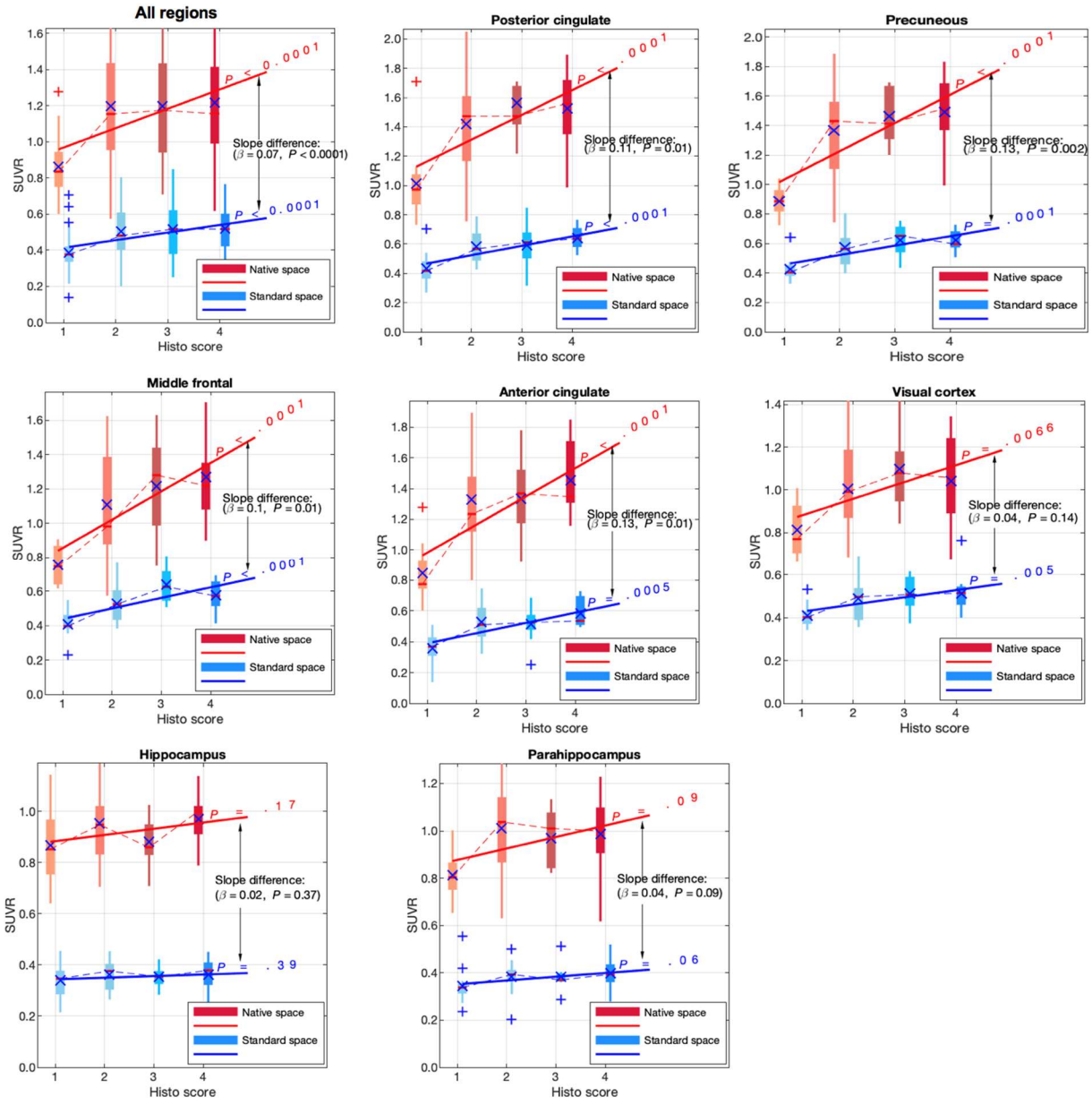

Supplemental Figure 1. Box and whisker plots with correlation and slope test parameters showing SUVR distribution obtained using native and standard method using FreeSurfer atlas in the MNI space template.